

3D Object Super-Resolution

Edward Smith
Department of Computer Science
McGill University
Montreal, Canada
edward.smith@mail.mcgill.ca

Scott Fujimoto
Department of Computer Science
McGill University
Montreal, Canada
scott.fujimoto@mail.mcgill.ca

David Meger
Department of Computer Science
McGill University
Montreal, Canada
dmeger@cim.mcgill.ca

Abstract—We consider the problem of scaling deep generative shape models to high-resolution. To this end, we introduce a novel method for the fast up-sampling of 3D objects in voxel space by super-resolution on the six orthographic depth projections. We demonstrate the training of object-specific super-resolution CNNs for depth maps and silhouettes. This allows us to efficiently generate high-resolution objects, without the cubic computational costs associated with voxel data. We evaluate our work on multiple experiments concerning high-resolution 3D objects, and show our system is capable of accurately increasing the resolution of voxelized objects by a factor of up to 16, to produce objects at resolutions as large as $512 \times 512 \times 512$ from $32 \times 32 \times 32$ resolution inputs. Additionally, we demonstrate our method can be easily applied in conjunction with the reconstruction of high-resolution objects from RGB images to achieve quantitative and qualitative state-of-the-art performance for this task.

I. INTRODUCTION

The physical world is made up of infinitely many structures of fine detail and texture that far surpass the limited bandwidth of robotic sensors and representational power of shape representations. In this paper, we seek to improve the ability of robots to interpret the detailed shape of objects that they interact with. Our approach builds upon deep generative models that have recently been shown to achieve human-like performance in hallucinating diverse 3D objects, capturing their overall shape and many structural elements. Popular deep generative approaches based on voxels, such as 3DGAN [38] scale poorly with resolution, in both computation and memory requirements, preventing generation of fine details. Super-resolution, the task of generating high-resolution structures from a low-resolution counterpart, is able to imagine the information which has been lost.

We propose a novel approach for deep shape interpretation and super-resolution, which is capable of generating the highest resolution models of any recent deep generative approach while also training more efficiently and achieving state-of-the-art qualitative and quantitative performance.

To overcome the cubic computational burden inherent in representing voxelized objects, we have developed a method to upscale the projections of 3D objects which can then be used to reconstruct a high-resolution voxelized object via space carving. We capture the full structure of an object by forming the orthographic depth projections corresponding to its six axis-aligned faces. An example of such projections can be viewed in figure 2. While multi-view representations of 3D objects

have been considered in prior work [26, 35], we combine these faces along with a low-resolution 3D representation of the object, allowing us to simultaneously capture fine-grained textures with volumetric information.

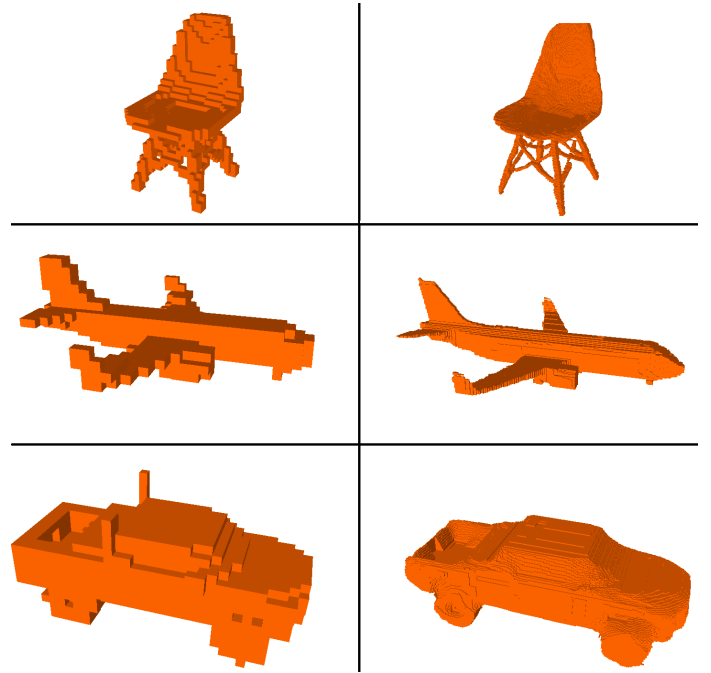


Fig. 1: Sample outputs of our 3D object super-resolution method (right), from corresponding low-res inputs (left) in the chair, plane and car object classes.

Our super-resolution method allows us to accurately predict high-resolution voxel objects from low-resolution inputs, with up to a 16 times increase in the resolution. Note that unlike classical smoothing-based methods for up-sampling, due to the data-driven nature of our approach, class specific details and properties are captured by the weights of the networks and can be accurately restored. We demonstrate the accuracy of our method quantitatively by examining the intersection over union (IoU) scores of predicted 256^3 objects from 32^3 object inputs when compared to ground truth for 3 object classes. To highlight the impressive visual quality our method boasts, we render multiple predicted 256^3 voxel objects across each class, and predicted 512^3 voxel objects across a chair object class.

We further demonstrate the effectiveness of our method

by combining it with a novel low-resolution 3D object reconstruction method to tackle the task of high-resolution 3D object reconstruction from single RGB images. We developed and trained a new deep convolutional autoencoder system to reconstruct voxelized objects at resolution 32^3 from 128×128 resolution images capturing objects at random viewpoint and lighting conditions. We then passed these objects through our super-resolution system to produce reconstructions at 256^3 resolution. We achieve state of the art IoU scores for this task. In addition, the objects produced using this combination of methods are visually impressive, both in isolation, and when compared to the ground truth objects. Code for all of our systems is publicly available on a GitHub repository, in order to ensure reproducible experimental comparison¹.

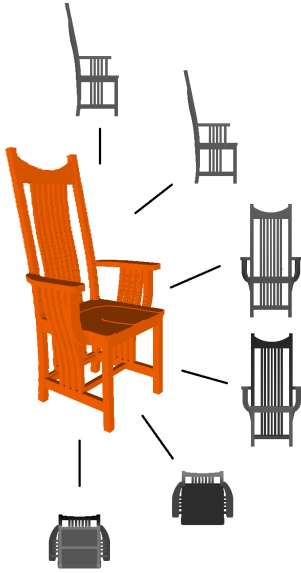


Fig. 2: A 256^3 resolution object surrounded by six axis-aligned orthographic depth maps.

II. RELATED WORKS

Super-Resolution The problem of super-resolution of 2D images is a well-studied problem [24]. Traditionally, image super-resolution has used dictionary-style methods [5, 40], matching patches of images to higher-resolution counterparts. This extends to depth-map super-resolution [18, 23, 10]. Modern approaches to super-resolution are built on deep convolutional networks [4, 37, 22] as well as generative adversarial networks [15, 36] which use an adversarial loss to imagine high-resolution details in RGB images.

Deep Learning with 3D Data Most recent advances with 3D data have leveraged deep learning, beginning with novel architectures such as 3D convolutions [20, 16] for object classification. Following advances in 2D image generation, generative adversarial network approaches have been used to generate novel 3D objects [38, 34, 17]. Deep learning has been used for 3D object reconstruction from a single image [3], by

embedding the image into learned representations [6] [39] or from generative modeling [38, 30].

Representations of 3D Data Given that naïve representations of 3D data require cubic computational costs with respect to resolution, many alternate representations have been proposed. Our work connects to multi-view representations which capture the characteristics of a 3D object from multiple viewpoints [14, 21, 35, 26], decomposing image silhouettes [19], Light Field Descriptors [2], or 2D panoramic mapping [31].

Other representations aim to use orientation [29], rotational invariance [11] or 3D-SURF features [13]. While many of these representations are effective for 3D classification, they reduce the dimensionality of the objects and capture insufficient detail for object reconstruction or super-resolution. Less structured alternate representations such as point clouds [27] or mesh models [25] have been used, however, these methods use unstructured representations and there is no readily available methodology for converting them into realistic 3D models. Hierarchical surface prediction [8] is a method which, like our work, uses an alternate representation to decrease computational costs. HSP divides the voxel space into free, occupied and boundary space, where the former two are disregarded. The object is generated at different scales of resolution, where occupied space is generated at a very coarse resolution and the boundary space is generated at a very fine resolution. While this does reduce the computational cost of generating high-resolution object, it still suffers from worst case cubic growth.

III. 3D OBJECT SUPER-RESOLUTION

In this section we describe our methodology for the super-resolution of 3D objects. Our algorithm is a novel approach for the semantic super-resolution of 3D objects represented as voxels. As shown in figure 3, rather than upscale voxels directly, we perform super-resolution by beginning with six low-resolution orthographic depth projections, which are up-sampled efficiently in 2D using deep networks trained to capture shape attributes specific to each object class. Finally, high-resolution depth maps and occupancy grids are smoothed and merged to recreate the 3D voxels of the object at a high-resolution. This approach is able to recover fine object details and scales well to higher resolutions than previous methods, due to the simplified learning problem faced by each network, and scalable computations that occur primarily in 2D.

A. Depth Map Orthographic Projections

We begin by obtaining the orthographic depth maps (ODM) of the six primary views of the low-resolution 3D object.

Each pixel (x, y) in an ODM holds the value d , the object's surface depth along the vector perpendicular to the ODM at point (x, y) . For clarity, figure 2 shows the a chair object along with each of its six ODMs. This projection can be computed quickly and easily from an axis-aligned 3D array via z-clipping. If no voxels are present along a vector then we record a depth of 0.

¹<https://github.com/EdwardSmith1884/3D-Object-Super-Resolution>

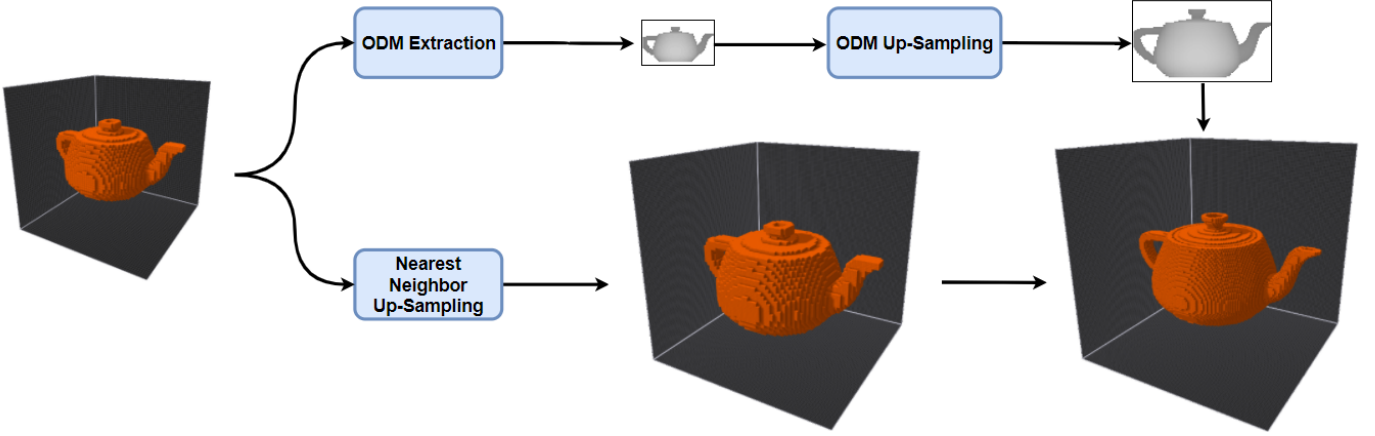


Fig. 3: A graphic outlining the stages and outputs of each step in our super-resolution framework.

B. Depth Map Upscaling

Super-resolution is an under-constrained problem since fine detail is entirely missing from low-resolution inputs. Restoring it accurately requires capturing object-specific shape attributes, and we train deep convolutional models to perform this task. In particular, we predict the ODM of the high-resolution object using a network that takes the corresponding ODM of the low-resolution object as input. This regularizes and reduces the complexity of the resulting learning problem, leading to improved results when compared with directly estimating new surface depths.

Given the true high-resolution depth map D_H is often close to the low-resolution input, we therefore limit our network’s output to a small range of relative depth values – a minor approximation that sacrifices little performance while allowing much more reliable and faster training. We create low-resolution 3D objects that contain the true object, requiring us to predict only positive depth changes. We will later discuss how this property is achieved during the training of our low-resolution object generator. In addition, we assume a maximum error bound for the low-resolution object, such that the depth change required is r , at maximum.

A caveat is that by bounding the networks ability to carve the surface, it is not able to completely remove all voxels along a given vector. It is important to allow this complete removal to take place, for example in instances where new holes or indentations of the outline should be created. To remedy this, we make a second prediction which outputs the expected high-resolution silhouette of the image, in the form of an occupancy map indicating where the object will be present in each ODM.

The low-resolution depth map D_L is passed through a deep convolution neural network, denoted SR with parameters θ , whose final input is passed through a sigmoid, to produce an estimate for the ODM within a fixed range, and added to the exactly up sampled low-resolution depth map to produce our prediction for a constrained high-resolution depth map CD_H :

$$CD_H = SR(D_L; \theta) + UP(D_L). \quad (1)$$

Where $UP(\cdot)$ up-samples using nearest neighbor interpolation and then multiplies the depth values in the result by the up-sampling factor. We constrain the output by using $r = 70$ for 256^3 objects and $r = 140$ for 512^3 objects

We train our network SR by minimizing the mean squared error with the ground truth high-resolution depth map, D_H . We further add a smoothing regularizer which penalizes the total variation TV [28] within the predicted ODM. Our loss function L is then defined by:

$$L(\theta) = \|CD_H - D_H\|^2 + \lambda TV(CD_H). \quad (2)$$

The total variation penalty is used as an edge-preserving denoising which smooths out irregularities in the output. An example output of this depth super-resolution procedure can be seen under figure 4 in image B).

The network M with parameters ϕ for the predicting the high-resolution occupancy map is passed the same low-resolution image as in the depth predictions. The network outputs a probability that each pixel is occupied. It is trained by minimizing the mean squared error between the predicted and true silhouettes,

$$L(\phi) = \|M(D_L; \phi) - \mathbb{1}_{D_H(i,j) \neq 0}(D_H)\|^2, \quad (3)$$

where $\mathbb{1}$ is the indicator function. An example output of this occupancy super-resolution procedure can be seen under figure 4 in image C). The output of the constrained depth map and occupancy map super-resolution networks are then combined to produce a complete prediction for the high-resolution ODM. This accomplished by masking the constrained high-resolution depth map by the predicted occupancy map after rounding,

$$\hat{D}_H = (SR(D_L; \theta) + UP(D_L)) \circ M(D_L; \phi), \quad (4)$$

where \circ is pairwise multiplication. An example output combination can be seen in figure 4 under image D).

The final step is then to smooth the resulting ODM with an adapted averaging filter of 5×5 pixels. To preserve edges only pixels within c of the original value are included, with $c = 10$ for 256^3 objects and $c = 20$ for 512^3 objects. This smoothing along with the total variation regularization in the our loss

function are added to avoid large changes in pixel value when the output of the constrained depth super-resolution network is added to the naïvely up-sampled low-resolution ODM. An example output of this smoothing can be seen under figure 4 in image E).

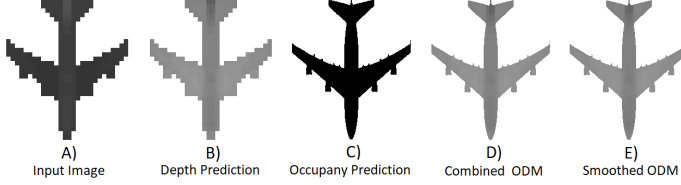


Fig. 4: This figure displays the various stages of our super-resolution pipeline. Image A) shows the input depth map for a single ODM. Image B) shows the predicted depth to carve into the face's surface. Image C) shows the predicted occupancy map for the ODM. Image D) shows the combination of images B) and C) into a rough prediction for the ODM's new surface. Image E) show our final prediction for the ODM's surface, after smoothing is applied to image D).

C. Model Carving

To complete our super-resolution procedure, the six ODMs are combined with the low-resolution object to form a high-resolution object. We first up-sample the low-resolution model to the desired resolution. This is accomplished in 3D using nearest neighbor interpolation. We then use our predicted ODMs to determine the surface of the new object. For each ODM, a pixel value $d > 0$, at position (x, y) indicates to remove all voxels found along the vector perpendicular that ODM at position (x, y) up to a depth of d . If the value d is 0 then all voxels are removed along that vector, if at least 2 ODMs agree on its removal. Due to the large amount overlap in surface area that the six ODMs observe, this silhouette agreement is enforced to increase the accuracy of the final object. However, we do not require agreement within the constrained depth map predictions. This is because, unlike the occupancy maps, a depth map can cause or deepen concavities in the surface of the object which may not be visible from any other face. Requiring agreement among depth maps eliminates their ability to influence these concavities.

D. Network Architecture

The networks used for predicting high-resolution depth maps and occupancy maps share the same architecture. This architecture is derived from the generator used by SRGAN [15]. It begins with a single convolutional layer followed by 16 identical residual blocks [9] with batch normalization, ReLU activations, and skip connections attaching each subsequent layer. This is followed by a convolutional layer with batch normalization, a ReLU activation function, and a skip connection attached to the output of the first convolutional layer. The final layers are a series of sub-pixel convolution layers as found in Shi et al. [32] and a final convolutional layer to decrease the color channel to 1, followed by a sigmoid activation to limit the output range. The number of sub-pixel convolution layers is equal to the \log_2 of the upscaling factor. The kernel size is 3×3 and stride length is 1 for all layers, and all convolutional layers have kernel depth 128 except for

the last, with depth 1. The kernel depth begins at size 256 for the sub-pixel convolutional layers and decreases by a factor of 2 for each subsequent layer, to offset the increase in kernel height and width.

IV. 3D OBJECT RECONSTRUCTION FROM A SINGLE IMAGE

In this section we describe our methodology for efficiently reconstructing a high-resolution voxelized object from a single RGB image. We outline a new system for reconstructing highly accurate voxelized 3D objects at low-resolution, which can be used with our 3D super-resolution to produce high-resolution object reconstructions. This process is described in figure 5.

A. Low-Resolution 3D Object Reconstruction

Recent results [3, 6] in 3D object reconstruction using deep autoencoders have shown to be effective at lower resolutions but are infeasible at higher resolutions due to cubic computational, memory, and parameter costs. To this end, we introduce a novel deep 3D convolutional autoencoder system to reconstruct objects from RGB images which are further upgraded by our super-resolution method. The autoencoder consists of an encoder inspired by the object reconstruction network in used in Smith and Meger [34], and a decoder inspired by the baseline decoder in HSP [8]. Together, they make up a simple convolutional autoencoder that is described in full detail in section IV-B.

The parameters θ of the autoencoder A was trained to minimize the mean squared error (MSE) and the mean absolute error (MAE) between the ground truth V and predicted 3D objects $A(x; \theta)$ from image inputs x ,

$$L(\theta) = \|V_i - A(x_i; \theta)\|^2 + \lambda |V_i - A(x_i; \theta)|. \quad (5)$$

As 3D object reconstruction is an imprecise task, we use a small ensemble of 5 autoencoders to remove noisy artifacts. While the use of ensembles increase training time, this is computationally feasible due to the simplicity of our architecture. For each possible position in our object space, a voxel was only voted to be present if 3 out of the 5 autoencoders output a value of greater than 0.45. While this does not necessarily return the lowest mean squared error, due to the nature of our super-resolution system, it is far more desirable to include a false voxel than to omit a true one.

Once the low-resolution object has been produced, it is passed through the super-resolution pipeline, outputting the predicted high-resolution object.

B. Network Architecture

The network used for predicting the low-resolution 3D objects is a deep convolutional autoencoder. The encoder network of this system takes as input a RGB image and passes it through 5 convolutional layers with batch normalization, leaky-ReLu activations, and stride length 2, followed by a fully connected layer to produce a vector of length 128.

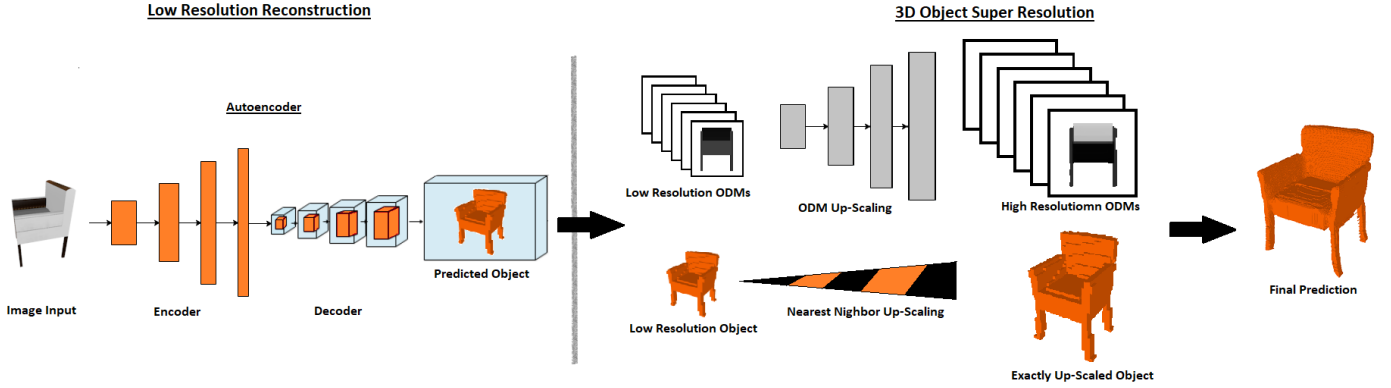


Fig. 5: The complete pipelines for our two methods outlined in this paper.

The network architecture for the decoder begins with a fully connected layer to increase the vector to length 1024 followed by an alternation of 9 3D deconvolutional and convolutional layers to morph the up-sampled vector to a complete 3D shape. It outputs a $32 \times 32 \times 32$ matrix of voxel probabilities.

V. EXPERIMENTS

A. Datasets

There are two main datasets used for our experiments. The first consists of 256^3 voxelized objects and their 32^3 counterparts. These objects were produced by converting CAD models found in the ShapeNetCore dataset [1] into voxel format. We chose 3 object classes from this dataset to experiment with: cars, chairs, and airplanes. For the chair class we also produce 512^3 voxel objects. For training, we preprocess this dataset, to extract the six ODMs from each object at high and low-resolution.

CAD models converted at this resolution do not remain watertight in many cases, making it difficult to fill the inner volume of the object. A method to fix this problem, suggested by Häne et al. [8], involves eroding one voxel across the entire surface of the lower resolution model, applying a nearest neighbor up-sampling to high-resolution, occupying all voxels that intersect with the mesh, and then applying a graph-cut based regularization with a small smoothness term to decide the remaining voxels. While this does rectify the issue of non watertight meshes, it may not reproduce the original surface perfectly and may lead to an overly smooth model.

We suggest a new method to produce accurate, high-resolution voxel models from non-watertight CAD models. We first convert the CAD model to voxels at resolution 256^3 , and determine their orthographic depth maps. The high-resolution models are then down-sampled to 32^3 resolution (wherein they are guaranteed to be watertight), then all internal voxels are filled, next they are up-sampled to the original resolution using nearest neighbor interpolation. Finally, the six depth faces are used to carve away the surface voxels of the reproduced high-resolution object. The only situation in which this does not make a complete model is in the rare case when the CAD model is missing one or more large faces at some point on

its surface, and these object are automatically discarded as no true voxel object can be extracted from the model.

The second dataset is used to reconstruct high-resolution objects from RGB images. This dataset re-uses the 32^3 and 256^3 objects produced for the previous dataset. The CAD models for each of these object were rendered into 10 128^2 RGB images capturing random viewpoints of the objects at elevations between $(-20^\circ, 30^\circ)$ and all possible azimuth rotations. The voxelized objects and corresponding images were split into a training, validation and test set, with a ratio of 70:10:20 respectively. This dataset perfectly mimics the dataset used to train and test the high-resolution object reconstructions used by HSP [8].

B. Analysis of Super-Resolution Method

Several state of the art super-resolution techniques were tested alongside our own system to compare accuracy on our task. The first was a slight variant on SRGAN [15], a state of the art adversarial generation system for image super-resolution, adept at producing photo-realistic RGB images at up to a 4 times resolution increase. The SRGAN system applies the generic GAN loss formulation [7] along side a VGG loss (based on the difference of of layer activations from a pre-trained VGG network [33]) to upscale images, equipped with two deep convolutional neural networks (CNNs) acting as their generator and discriminator. The VGG loss term was removed from the generator loss function, and replaced by MSE loss as our dataset is far more constrained.

The second super-resolution algorithm compared was the SRGAN algorithm without adversarial loss. This corresponds to the generator of SRGAN directly predicting the higher resolution image, trained with a MSE loss. This was used as the adversarial loss is employed to achieve photorealism rather than reconstruction accuracy.

The third super-resolution scheme tested for our task was MS-Net [10], the state of the art for depth map super-resolution. This passes depth maps through a CNN consisting of a convolutional layer followed by, 3 deconvolution networks to increase the image dimensionality, then culminating in a final convolutional layer to output the high-resolution image. The novelty in the scheme is that instead of passing the image

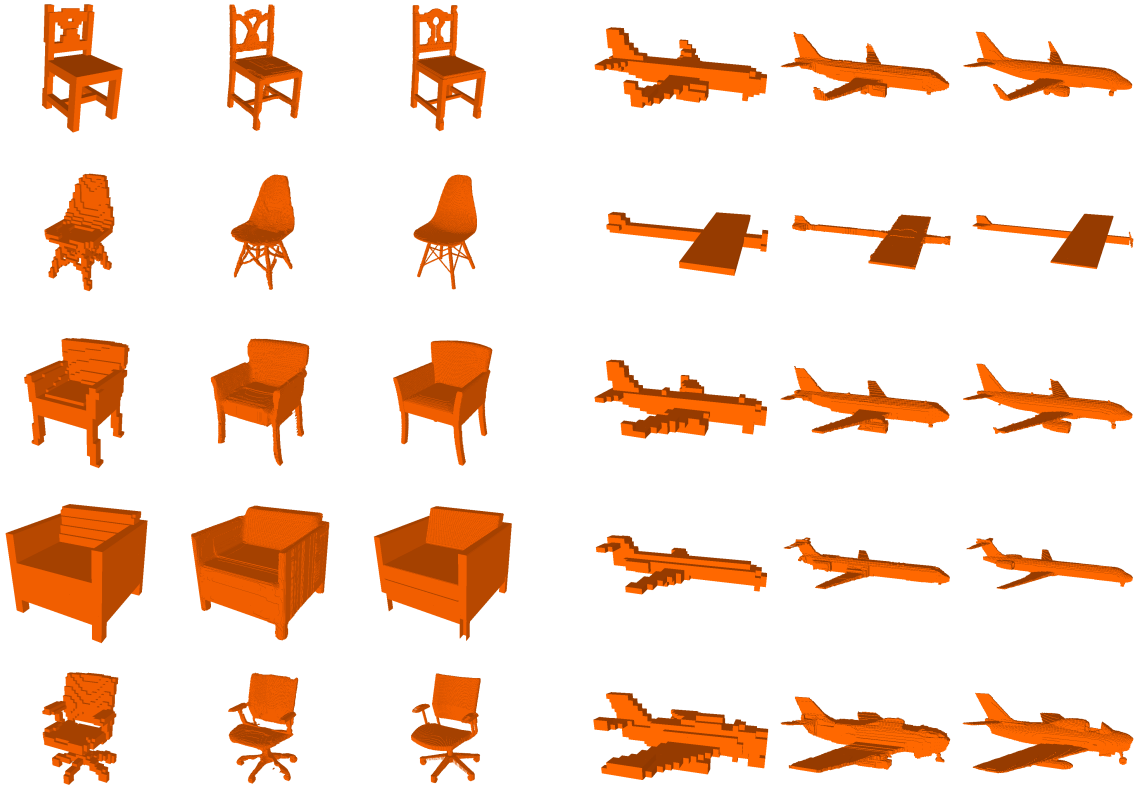


Fig. 6: Super-resolution results from 32^3 resolution to 256^3 resolution from objects found in the chair and plane class of the ShapeNet Dataset. For each object class, the left image corresponds to the low-resolution input, the middle image our reconstruction result, and the right image is the ground truth object.

directly, only the high frequency details are passed through the network, and the result is the added to the original images low frequency information which is up-sampled to the higher resolution using bi-cubic interpolation.

We compare the accuracy of these algorithms to our own by testing their performance at recovering 256^2 ODMs from 32^2 ODMs from the chair object class. We also test the performance of our algorithm when omitting smoothing, not including our information from the occupancy maps, and when not including information from the depth maps. We train, validate, and test on the same 70:10:20 split as for the image reconstruction task. We trained all networks using the Adam optimizer [12] with a learning rate of 10^{-4} , and halted learning when the performance IoU score on the validation set tested every epoch, bottomed out. The MSE for each algorithm on our held-out test set is shown in table I As can be seen, our algorithm achieves far lower error when recovering ODMs. It can also be seen here that smoothing and depth map information all play a role in improving the accuracy of our algorithm.

C. 3D Object Super-Resolution

To qualitatively demonstrate the results of our super-resolution system we rendered 5 randomly selected results from each object class test set. These results are shown in

TABLE I: Super-Resolution Mean Squared Error

Method	MSE
SRGAN [15]	1268.53
SRGAN Generator [15]	919.64
MS-Net [10]	1659.89
3D-OSR without depth map (Ours)	813.28
3D-OSR without smoothing (Ours)	745.72
3D-OSR (Ours)	712.25

TABLE II: Super-Resolution IoU

Method	Car	Chair	Airplane
N.N Up-Sampling	67.7	54.9	39.9
3D-OSR, Occupancy Map Only	79.3	67.3	70.2
3D-OSR	80.4	68.5	71.1

figure 6 for the chair and plane classes, figure 7 for the car class. The predicted high-resolution objects are all of high quality and accurately mimic the features of the ground truth objects. We can also observe in these figures, along with the image E) in figure 4, that due to the data-driven nature of our method, class specific features and properties arise.

To further validate the power of our algorithm we trained new networks to perform super-resolution from 32^3 to 512^3 on the chair class. We qualitatively evaluated our performance

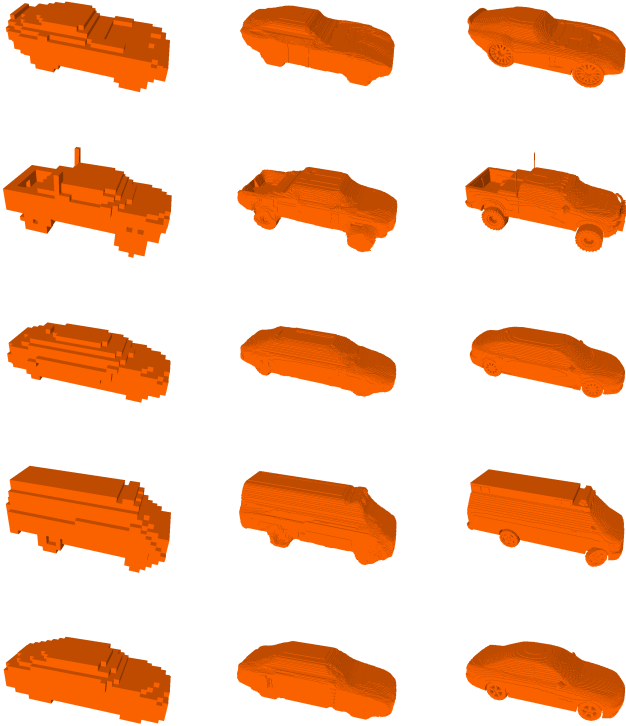


Fig. 7: Super-resolution results from 32^3 resolution to 256^3 resolution from objects found in the car class of the ShapeNet Dataset. For each object, the left image corresponds to the low-resolution input, the middle image our reconstruction result, and the right image is the ground truth object.

on the test set, and verified the algorithm is still able to perform well, even at a 16 times increase. To demonstrate this performance we rendered our best 3 objects out of the first 10 predicted objects viewed. These objects are displayed in figure 8, alongside their corresponding low-resolution objects and high-resolution ground truth.

D. 3D object Reconstruction from RGB Images

TABLE III: Single Image Object Reconstruction IoU

Method	Car	Chair	Airplane
HSP [15]	70.1	37.8	56.1
Ours	72.7	40.1	56.4

To test the performance of our 2D to 3D object reconstruction algorithm, we first trained our ensemble of 5 autoencoders to produce objects at 32^3 resolution, in each object class. We trained each autoencoder separately, first using a learning rate of 10^{-4} and then fine-tuning at a learning rate of 10^{-5} . Training was performed using the Adam optimizer and was halted when the IoU scores on the validation set stopped decreasing. We combined the output of these 5 models by only placing a voxel in a position if 3 or more of the ensembles predicted a value of greater than 0.45 in that position. This method was arrived at through experimentation on the validation set. We then applied our super-resolution

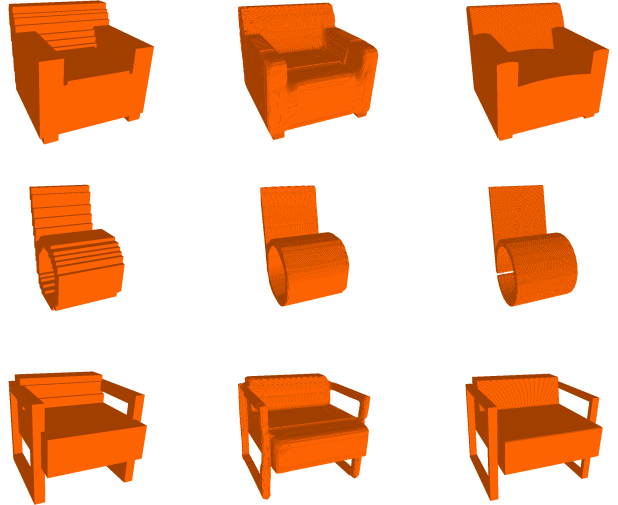


Fig. 8: Super-resolution results from 32^3 resolution to 512^3 resolution from objects found in the chair class of the ShapeNet Dataset. For each object, the left image corresponds to the low-resolution input, the middle image our reconstruction result, and the right image is the ground truth object.

method to the low-resolution models to produce 256^3 models. We evaluated our performance at this task by computing our IoU scores on the test set for each object class.

Our results compared to HSP [8] can be seen in table III. We achieve state-of-the-art performance on every object class. To qualitatively evaluate our performance, we rendered our reconstructions for each class. A purposefully varied selection of these renderings can be seen in figure 9. In these figures also display the input image and the ground truth object for fair evaluation.

VI. CONCLUSION

In this paper we outline a novel system for increasing the resolution of 3D objects while capturing their category-specific shape details. This is achieved through the application of a novel super-resolution system that operates over the six orthographic projections of the object. Our method outperforms the baseline method in IoU by a large margin. We further demonstrate the high accuracy of this up-sampling procedure with up to a 16 times increase in size, up to a 512^3 resolution, producing visually impressive results, even when compared to the ground truth. We then apply this system to the reconstruction of high-resolution 3D objects from single RGB images, and achieve state of the art results after applying our super resolution algorithm to the low-resolution reconstructions. Given that the deep aspect of our method works entirely in 2D space, our method scales naturally to high-resolutions, and all of our computations were run on a single NVIDIA Titan X GPU.

REFERENCES

- [1] Angel X Chang, Thomas Funkhouser, Leonidas Guibas, Pat Hanrahan, Qixing Huang, Zimo Li, Silvio Savarese, Manolis Savva, Shuran Song, Hao Su, et al. Shapenet:

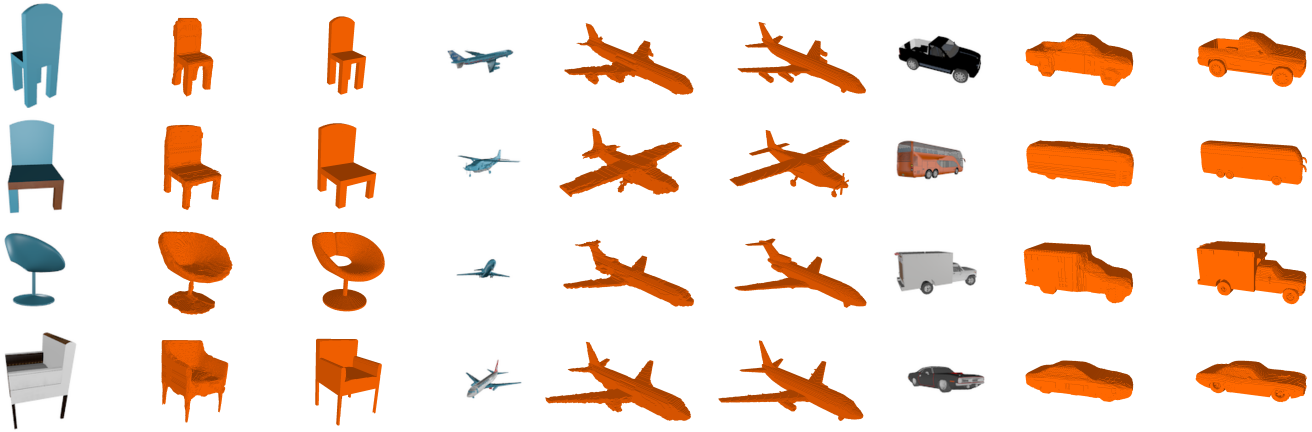


Fig. 9: Reconstruction results on the ShapeNet Dataset with our super-resolution system. The left image for each class is the 2D input image, the middle image our 3D reconstruction result, and the right image the 3D ground truth image.

- An information-rich 3d model repository. *arXiv preprint arXiv:1512.03012*, 2015.
- [2] Ding-Yun Chen, Xiao-Pei Tian, Yu-Te Shen, and Ming Ouhyoung. On visual similarity based 3d model retrieval. In *Computer graphics forum*, volume 22, pages 223–232. Wiley Online Library, 2003.
 - [3] Christopher B Choy, Danfei Xu, JunYoung Gwak, Kevin Chen, and Silvio Savarese. 3d-r2n2: A unified approach for single and multi-view 3d object reconstruction. In *European Conference on Computer Vision*, pages 628–644. Springer, 2016.
 - [4] Chao Dong, Chen Change Loy, Kaiming He, and Xiaoou Tang. Image super-resolution using deep convolutional networks. *IEEE transactions on pattern analysis and machine intelligence*, 38(2):295–307, 2016.
 - [5] William T Freeman, Thouis R Jones, and Egon C Pasztor. Example-based super-resolution. *IEEE Computer graphics and Applications*, 22(2):56–65, 2002.
 - [6] Rohit Girdhar, David F Fouhey, Mikel Rodriguez, and Abhinav Gupta. Learning a predictable and generative vector representation for objects. In *European Conference on Computer Vision*, pages 484–499. Springer, 2016.
 - [7] Ian Goodfellow, Jean Pouget-Abadie, Mehdi Mirza, Bing Xu, David Warde-Farley, Sherjil Ozair, Aaron Courville, and Yoshua Bengio. Generative adversarial nets. In *Advances in neural information processing systems*, pages 2672–2680. 2014.
 - [8] Christian Häne, Shubham Tulsiani, and Jitendra Malik. Hierarchical surface prediction for 3d object reconstruction. 2017.
 - [9] Kaiming He, Xiangyu Zhang, Shaoqing Ren, and Jian Sun. Deep residual learning for image recognition. In *Proceedings of the IEEE conference on computer vision and pattern recognition*, pages 770–778, 2016.
 - [10] Tak-Wai Hui, Chen Change Loy, and Xiaoou Tang. Depth map super-resolution by deep multi-scale guidance. pages 353–369, 2016.
 - [11] Michael Kazhdan, Thomas Funkhouser, and Szymon Rusinkiewicz. Rotation invariant spherical harmonic representation of 3 d shape descriptors.
 - [12] Diederik P Kingma and Jimmy Ba. Adam: A method for stochastic optimization. *arXiv preprint arXiv:1412.6980*, 2014.
 - [13] Jan Knopp, Mukta Prasad, Geert Willems, Radu Timofte, and Luc Van Gool. Hough transform and 3d surf for robust three dimensional classification. In *European Conference on Computer Vision*, pages 589–602. Springer, 2010.
 - [14] Jan J Koenderink and Andrea J Van Doorn. The singularities of the visual mapping. *Biological cybernetics*, 24(1):51–59, 1976.
 - [15] Christian Ledig, Lucas Theis, Ferenc Huszár, Jose Caballero, Andrew Cunningham, Alejandro Acosta, Andrew Aitken, Alykhan Tejani, Johannes Totz, Zehan Wang, et al. Photo-realistic single image super-resolution using a generative adversarial network. *arXiv preprint arXiv:1609.04802*, 2016.
 - [16] Yangyan Li, Soeren Pirk, Hao Su, Charles R Qi, and Leonidas J Guibas. Fpnn: Field probing neural networks for 3d data. In *Advances in Neural Information Processing Systems*, pages 307–315, 2016.
 - [17] Jerry Liu, Fisher Yu, and Thomas Funkhouser. Interactive 3d modeling with a generative adversarial network. *arXiv preprint arXiv:1706.05170*, 2017.
 - [18] Oisín Mac Aodha, Neill DF Campbell, Arun Nair, and Gabriel J Brostow. Patch based synthesis for single depth image super-resolution. In *European Conference on Computer Vision*, pages 71–84. Springer, 2012.
 - [19] Diego Macrini, Ali Shokoufandeh, Sven Dickinson, Kaleem Siddiqi, and Steven Zucker. View-based 3-d object recognition using shock graphs. In *Pattern Recognition, 2002. Proceedings. 16th International Conference on*, volume 3, pages 24–28. IEEE, 2002.
 - [20] Daniel Maturana and Sebastian Scherer. Voxnet: A 3d convolutional neural network for real-time object

- recognition. In *Intelligent Robots and Systems (IROS), 2015 IEEE/RSJ International Conference on*, pages 922–928. IEEE, 2015.
- [21] Hiroshi Murase and Shree K Nayar. Visual learning and recognition of 3-d objects from appearance. *International journal of computer vision*, 14(1):5–24, 1995.
- [22] Christian Osendorfer, Hubert Soyer, and Patrick Van Der Smagt. Image super-resolution with fast approximate convolutional sparse coding. In *International Conference on Neural Information Processing*, pages 250–257. Springer, 2014.
- [23] Jaesik Park, Hyeonwoo Kim, Yu-Wing Tai, Michael S Brown, and Inso Kweon. High quality depth map upsampling for 3d-tof cameras. In *Computer Vision (ICCV), 2011 IEEE International Conference on*, pages 1623–1630. IEEE, 2011.
- [24] Sung Cheol Park, Min Kyu Park, and Moon Gi Kang. Super-resolution image reconstruction: a technical overview. *IEEE signal processing magazine*, 20(3):21–36, 2003.
- [25] Jhony K Pontes, Chen Kong, Sridha Sridharan, Simon Lucey, Anders Eriksson, and Clinton Fookes. Image2mesh: A learning framework for single image 3d reconstruction. *arXiv preprint arXiv:1711.10669*, 2017.
- [26] Charles R Qi, Hao Su, Matthias Nießner, Angela Dai, Mengyuan Yan, and Leonidas J Guibas. Volumetric and multi-view cnns for object classification on 3d data. In *Proceedings of the IEEE conference on computer vision and pattern recognition*, pages 5648–5656, 2016.
- [27] Charles R Qi, Hao Su, Kaichun Mo, and Leonidas J Guibas. Pointnet: Deep learning on point sets for 3d classification and segmentation. *Proc. Computer Vision and Pattern Recognition (CVPR), IEEE*, 1(2):4, 2017.
- [28] Leonid I Rudin, Stanley Osher, and Emad Fatemi. Nonlinear total variation based noise removal algorithms. *Physica D: nonlinear phenomena*, 60(1-4):259–268, 1992.
- [29] Ashutosh Saxena, Min Sun, and Andrew Y Ng. Make3d: Learning 3d scene structure from a single still image. *IEEE transactions on pattern analysis and machine intelligence*, 31(5):824–840, 2009.
- [30] Abhishek Sharma, Oliver Grau, and Mario Fritz. Vconv-dae: Deep volumetric shape learning without object labels. In *European Conference on Computer Vision*, pages 236–250. Springer, 2016.
- [31] Baoguang Shi, Song Bai, Zhichao Zhou, and Xiang Bai. Deeppano: Deep panoramic representation for 3-d shape recognition. *IEEE Signal Processing Letters*, 22(12):2339–2343, 2015.
- [32] Wenzhe Shi, Jose Caballero, Ferenc Huszár, Johannes Totz, Andrew P Aitken, Rob Bishop, Daniel Rueckert, and Zehan Wang. Real-time single image and video super-resolution using an efficient sub-pixel convolutional neural network. pages 1874–1883, 2016.
- [33] Karen Simonyan and Andrew Zisserman. Very deep convolutional networks for large-scale image recognition. *arXiv preprint arXiv:1409.1556*, 2014.
- [34] Edward J. Smith and David Meger. Improved adversarial systems for 3d object generation and reconstruction. In *Proceedings of the 1st Annual Conference on Robot Learning*, volume 78 of *Proceedings of Machine Learning Research*, pages 87–96. PMLR, 13–15 Nov 2017.
- [35] Hang Su, Subhransu Maji, Evangelos Kalogerakis, and Erik Learned-Miller. Multi-view convolutional neural networks for 3d shape recognition. In *Proceedings of the IEEE international conference on computer vision*, pages 945–953, 2015.
- [36] Samuli Laine Jaakko Lehtinen Tero Karras, Timo Aila. Progressive growing of gans for improved quality, stability, and variation. *International Conference on Learning Representations*, 2018.
- [37] Zhaowen Wang, Ding Liu, Jianchao Yang, Wei Han, and Thomas Huang. Deep networks for image super-resolution with sparse prior. In *Proceedings of the IEEE International Conference on Computer Vision*, pages 370–378, 2015.
- [38] Jiajun Wu, Chengkai Zhang, Tianfan Xue, William T Freeman, and Joshua B Tenenbaum. Learning a probabilistic latent space of object shapes via 3d generative-adversarial modeling. In *Advances in Neural Information Processing Systems*, pages 82–90, 2016.
- [39] Xinchun Yan, Jimei Yang, Ersin Yumer, Yijie Guo, and Honglak Lee. Perspective transformer nets: Learning single-view 3d object reconstruction without 3d supervision. In *Advances in Neural Information Processing Systems*, pages 1696–1704, 2016.
- [40] Jianchao Yang, John Wright, Thomas S Huang, and Yi Ma. Image super-resolution via sparse representation. *IEEE transactions on image processing*, 19(11):2861–2873, 2010.